Published in final edited form as:
Magn Reson Med. 2008 September ; 60(3): 749–760. doi:10.1002/mrm.21675.

3D High Temporal and Spatial Resolution Contrast-Enhanced MR Angiography of the Whole Brain

Clifton R. Haider, **Houchun Harry Hu, Ph.D.**, **Norbert G. Campeau, M.D.**, **John Huston III, M.D.**, and **Stephen J. Riederer, Ph.D.**
MR Research Laboratory, Mayo Clinic, Rochester, MN 55905

Abstract

Sensitivity encoding (SENSE) and partial Fourier techniques have been shown to reduce the acquisition time and provide high diagnostic image quality. However, for time-resolved acquisitions there is a need for both high temporal and spatial resolution. View sharing can be used to provide an increased frame rate but at the cost of acquiring spatial frequencies over a duration longer than a frame time. In this work, we hypothesize that a CArtesian Projection Reconstruction-like (CAPR) technique in combination with 2D SENSE, partial Fourier, and view sharing can provide 1 to 2 mm isotropic resolution with sufficient temporal resolution to distinguish intracranial arterial and venous phases of contrast passage in whole-brain angiography. In doing so, the parameter of "temporal footprint" is introduced as a descriptor for characterizing and comparing time-resolved view-shared pulse sequences. It is further hypothesized that short temporal footprint sequences have higher temporal fidelity than similar sequences with longer temporal footprints. The tradeoff of temporal footprint and temporal acceleration is presented and characterized in numerical simulations. Results from 11 whole-brain CE-MRA studies with the new method with SENSE acceleration factors R = 4 and 5.3 are shown to provide images of comparable or higher diagnostic quality than the unaccelerated reference.

Keywords

Contrast-enhanced MR Angiography; 2D-SENSE; 2D-partial Fourier; Temporal Footprint; View Sharing

INTRODUCTION

Since its initial description over a decade ago (1) three-dimensional (3D) contrast-enhanced MR angiography (CE-MRA) has become a widely used technique (2,3). Over the interim the method has undergone a number of technical advances allowing improved spatial and temporal resolution, including reduction of TR times, altered view orders to allow extended acquisition times (4), means for timing the acquisition to the arterial phase (5–7), development of stack of stars and 3D projection reconstruction (PR) techniques with application to MRA (8,9), and use of partial Fourier acquisition (10). More recently, parallel imaging methods (11–14) have been applied to 3D CE-MRA (15–23). A number of these methods can be applied synergistically.

Along with improvements in spatial resolution, there has been progress in the generation of time-resolved 3D CE-MRA data sets. This can be done by simply recycling an unaccelerated 3D pulse sequence (24,25) or by using view sharing to provide an image update rate shorter

Correspondence: Stephen J. Riederer, Ph.D., MR Research Laboratory, Mayo Clinic, 200 First Street, SW, Rochester, MN, 55905, Phone: 507-284-6209, Email: riederer@mayo.edu.

than the intrinsic acquisition time (26–28). Other versions of these methods have been developed (29–36), including use of such techniques as projection reconstruction (37) and spiral acquisition (38). Also, a method based on view-shared PR and slice encoding combined with non-linear processing has been developed for time-resolved imaging (39). A number of these methods for time-resolved MRA have been integrated with the above-mentioned parallel imaging for either improved temporal or spatial resolution. Applying parallel imaging along one dimension has been used to provide acceleration factors as high as 3 to 4 for time-resolved sequences (11,16,18,32,40–42). However, it has been shown for SENSE that for a given acceleration factor, 2D acceleration has markedly less SNR penalty than 1D (13). To our knowledge the first applications of 2D parallel imaging to time-resolved CE-MRA were presented in early 2006 (43–45) with other works presented subsequently (35,36).

This present work is an expansion of abstract (45). In developing and evaluating this method it was desirable to target an application having simultaneous demands for both high spatial and high temporal resolution. Thus, the principal hypothesis of this work was that a MR angiographic pulse sequence implementing these acceleration techniques would be able to temporally resolve the arterial and venous phases of the vasculature of the whole brain with resolution in the range of 1 to 2 mm isotropic. This was tested in two specific hypotheses to be presented. In the next sections the acquisition technique is described, simulations are presented which demonstrate the temporal fidelity of the sequence, and experimental results are presented from *in vivo* vascular studies of the brain. In doing so, the parameter of "temporal footprint" is also introduced for characterizing time-resolved view-shared sequences.

METHODS

Description of the Basic Sequence

The 3D time-resolved technique described here is based on a sampling pattern previously developed for non-time-resolved imaging (46) in which partial Fourier acquisition is performed across the 2D k_Y–k_Z phase encoding plane. This is shown schematically in Fig. 1A. Each point of the rectilinear grid of points shown represents a possible repetition of the experiment. When such a point is sampled, it is done with a full echo along the frequency encoding direction, normal to the plane of the figure. Each point within the central orange region is sampled in the acquisition. Outside this disk is an annulus composed of black vanes asymmetrically placed about the k_Y–k_Z origin. Underlying grid points lying within the black vanes are sampled; those points in the annular region but lying between the black vanes are not sampled. Signal values at these unsampled points are estimated from the sampled points using homodyne processing (47). The time order by which the sampled points are interrogated in the pulse sequence is arbitrary, but for CE-MRA the elliptical centric (EC) view order (48) is often used. The timing for this is shown schematically in Fig. 1B, where the orange central region is read out first, followed by the samples contained within the black vanes.

The sampling pattern of Fig. 1A was adapted in this work for time-resolved imaging as follows. The entire set of samples of Fig. 1A is repetitively sampled, but the central, fully-sampled region is sampled more frequently than the outer, annular region. The differential sampling rate between the central disk and outer annulus is created by sub-dividing the vanes within the annulus into groups. The frame rate, or rate at which image reconstruction is performed, is chosen to match the sampling rate of the central region. This is shown in Fig. 1D in which there are four groups and all vanes within a group are designated with a specific color: black, green, blue, red. This four-group decomposition is designated in this work as "N4." The timing diagram for the sequence is shown schematically in Fig. 1E. The sequence starts with sampling of the views lying within the central orange disk using the EC order. After the central orange disk is fully sampled the sampling continues immediately to those views lying within the black vanes of the annular region, again maintaining the EC order. The vanes within a group are

intentionally chosen to span the entire 2π radians azimuthally in order to impart minimal directional dependence to the point spread function within the y–z plane (49). After all views within the black vanes have been sampled the process starts over, and all views within the central orange disk are resampled. Upon completing a second sampling of the central orange disk a different group of vanes is sampled, in this case green as in (Fig. 1E), and again following the EC view order. The process continues for the blue and red vane sets as well, at which point the entire sampling cycle is repeated. Because CArtesian sampling is used but with a Projection Reconstruction-like pattern of spokes in the phase encoding plane, in the remainder of the work we refer to this sequence as "CAPR."

The use of the acquired N4 data for image reconstruction is illustrated in Fig. 2. Fig. 2A schematically shows contrast bolus time intensity profiles as measured in the carotid artery and jugular vein at the level of the carotid bifurcations. Fig. 2B shows the playout of views described in Fig. 1D, extended over multiple sampling cycles. Fig. 2C shows the subset of data from Fig. 2B used to form the first image frame. To sample all desired k-space points of Fig. 1D it is necessary to include samplings of all four colored frames and at least one central orange disk region. Because the central disk is measured four times more frequently than any annular vane group, there is a choice in which disk to use. However, to exploit the EC view order, the orange disk measured at the outset is selected. Because an image formed from the EC view order is dominated by the object status at the outset of the scan, the image reconstructed in Fig. 2C is assigned to the time indicated with the short vertical arrow shown.

Description of Temporal Footprint

In an effort to define an objective measure which can be used to characterize the extent of data acquisition used in time-resolved view-shared sequences, we propose the parameter of "temporal footprint." This is defined as the duration over which any views used for a single image are acquired. In the sequence described above this is equal to the time spent in sampling the four colored vane sets and four samplings of the central orange disk. This is indicated in the timing diagrams of Fig. 1 and in Fig. 2F. Because the sampling rate of the central zone is higher than of the annular region, the temporal footprint is larger than the acquisition time required to sample each k-space view only once. Data selection for subsequent frames in the sequence is shown in Figs. 2D–F. For each case the temporal footprint is the same duration as that of the first frame Fig. 2C and the central orange disk is sampled at the outset, preserving the centric nature for each individual timeframe.

Alternative View Orders

It may be desirable for some applications to use an alternative view order. A reverse elliptical centric (REC) order is defined as the time reversal of an EC order. In this case the views are sampled in the order of the outermost k-radius inward for each vane set and the central disk. This is shown schematically in Fig. 1C and Fig. 1F. In this case the temporal footprint of the sequence is identical to that for the EC case of Fig. 1B and Fig. 1E, respectively. However of the four samplings of the central disk region of k-space within the footprint, the last is used for image formation, and the time point to which the reconstructed image frame is assigned is at the end of the footprint. The REC order can be useful for real-time applications because the central k-space data have been acquired as close in time as possible to the instant the reconstruction process is initiated, thus minimizing any intrinsic latency between the temporal status of the object and the reconstructed image (50).

Alternative Frame Rates

The CAPR sequence as described can be readily adapted to provide different frame rates. This is done by subdividing the sampled vanes in the outer annulus into different numbers of groups other than four. Use of eight vane sets, designated “N8,” is illustrated in Figs. 1G. The eight

sets are again individually color coded, each now comprised of four individual vanes spanning 2π radians. The temporal playout using an EC view order is shown in Fig. 1H. The sampling follows that described for Fig. 1E and assumes as before that reconstruction is performed at the same rate as sampling of the central disk region. The frame rate is improved vs. Fig. 1E, but this is offset by an increase in the overall temporal footprint. Within this footprint any individual image contains data from only the first of the eight central samplings.

Incorporation of 2D SENSE

The Cartesian sampling pattern within the k_Y–k_Z plane lends itself to parallel acquisition, as previously shown for the non-time-resolved case with 2D SENSE (21). This is done for the time-resolved sequence of Fig. 1D by simply increasing the spacing along the k_Y and k_Z samples by respective acceleration factors R_Y and R_Z. The net acceleration R is equal to the product $R_Y \times R_Z$. This is shown schematically in Fig. 1I for two-fold accelerations along both Y and Z. Because the number of underlying grid points is reduced, so are the sampling durations of the central disk region and vane sets. This is reflected in the timing diagram of Fig. 1J. Because of the specific manner of sampling the central disk and vanes, the temporal footprint is reduced by less than a factor of four. Nonetheless, the reduction of the temporal footprint and the increase in the image frame rate for the same spatial resolution can be substantial.

Interplay Between Frame Rate, Temporal Footprint, and Acceleration

The interplay between image frame rate, temporal footprint, and acceleration provided by parallel imaging is shown in Fig. 3, which shows a plot of the temporal footprint vs. the image update time. Each curve corresponds to a different degree of acceleration as provided by parallel acquisition. The outermost curve of Fig. 3 corresponds to the specific sampling used in the experimental implementation of CAPR for the unaccelerated case. Referring to Fig. 1A, the full Cartesian sampling corresponds to 128 (k_Y) × 64 (k_Z) samples. The sampling distances along k_Y and k_Z are 1/(25.0 cm) and 1/(12.8 cm), respectively. The central disk region contains 90 points. The total number of sampled points including the central disk and all 32 vanes is 3174. For all cases shown in Fig. 3 it is assumed that the vane pattern provides two-fold net undersampling of the outer annular region, as shown for all k-space diagrams in Fig. 1, and homodyne reconstruction is performed. Changes in sampling from the 128 × 64 assumed would scale the curves of Fig. 3 proportionately.

The right endpoint of the outermost curve of Fig. 3 corresponds to the non-view-shared case, Fig. 1B. All vanes of the outer annulus are contained within one group, and this point is labeled “N1” in Fig. 3. Moving to the left along this curve corresponds to increased degrees of view sharing from one reconstructed frame to the next. The point labeled “N4” corresponds to the four-group case Figs. 1D–E, with subsequent points corresponding to increased numbers of vane groups. The middle and innermost curves of Fig. 3 correspond to the same extent of k-space sampling as the outermost curve but with assumed SENSE accelerations of R = 2 and R = 4, respectively. Note the radical reduction in both temporal footprint and image update time provided by parallel imaging. The maximum point of curvature on the operating curve also provides a practical tradeoff between a small image update time and the temporal footprint.

Simulations

Numerical phantom experiments were performed to assess the temporal fidelity of the CAPR technique to simulated contrast enhancement of the vasculature. For this purpose, a reference carotid enhancement pattern was measured *in vivo* at the level of the carotid bifurcation with an image update time of 1.75 sec and a temporal footprint of 7 sec. The vasculature of the numerical phantom consisted of one vessel 1.5 cm in diameter oriented along the frequency encoding direction. Signal level within an axial section through the vessel, lying within the y–z plane, was simulated. To simulate time-resolved acquisition the Fourier transform of the

vessel phantom was taken along the y–z directions. Next, the individual measurements were weighted on a TR by TR basis using the linearly interpolated arterial enhancement curve, and seeded into k_Y–k_Z space according to the view order and sampling pattern used. A 2D Fourier transform was then taken. The simulated signal level was taken to be the average measured value of a cross sectional region of interest covering the vessel in the y–z plane and plotted using the assumed time point for the dataset; i.e. the start or end of the temporal footprint for EC and REC view-orders, respectively. The resultant signal curve obtained from each CAPR simulation was then compared with the original arterial signal to determine temporal fidelity. This approach was used to study several aspects of the CAPR sequence: (i) unaccelerated CAPR versus R=2 1D and R=4 2D SENSE-accelerated CAPR acquisitions; (ii) EC versus REC view orders; and (iii) image update time versus temporal footprint in R=4 2D SENSE accelerated imaging. Detailed descriptions of the CAPR sequences used in simulations are shown in Table 1.

In Vivo Experiments

Time-resolved CE-MRA studies using the CAPR sequence were performed in human subject volunteers at 1.5T and 3.0T (GE Signa, Version 12.0 Excite) according to a protocol approved by our institutional review board. The typical scan parameters were: 3D spoiled gradient echo (GRE) sequence using TR/TE of 3.8/1.2 msec; flip angle 30°; BW ±62.5 kHz; sampling matrix 256 (S/I, frequency), 48–96 (A/P, phase), 32–64 (R/L slice); FOV of 25 cm (S/I and A/P) and 12–24 cm (R/L); and typical 2 min. in duration. It was useful to restrict the FOV along both the readout and the slice select directions precisely to the anatomy of interest, as facilitated by the 3DFT nature of the sequence. At both field strengths a similar eight-element head coil (MRI Devices, Waukesha, WI) was used. For all studies, 20 ml of gadobenate dimeglumine agent (MultiHance; Bracco Diagnostics, Princeton, NJ) was administered using an electronic injector into the right antecubital vein at 3 ml/sec followed by 20 ml of saline at 2 ml/sec. The last contrast-free frame was taken as the mask for subtraction of any background signal. 2D SENSE accelerations were typically performed using $R_Y = 2 – 2.67$ and $R_Z = 2$, yielding net acceleration factors R = 4 – 5.33. SENSE unfolding coefficients were obtained using a full resolution calibration scan consisting of a sagittal GRE pulse sequence with TR/TE 10/3 ms, flip angle = 10°, NEX = 1, and a bandwidth of ±31.25 kHz acquired prior to contrast injection and scaled by the sum of squares composite image of all coils. Acquisition parameters of *in vivo* studies are also given in Table 1.

Specific Hypotheses

In addition to performing *in vivo* studies for development of the CAPR sequence, two specific hypotheses were tested. The first hypothesis (H1) was: a four-fold SENSE-accelerated CAPR sequence can better portray the temporal passage of the contrast bolus through the brain vasculature than a similar unaccelerated sequence while still retaining adequate image quality. Because of the rapid transit of the contrast bolus through the brain, this is a more stringent test then, say, distinguishing contrast enhancement in the carotid artery bifurcation vs. the jugular vein. This hypothesis was tested in a six consecutive volunteers using sequences defined in Table 1 as Acq. 10 and Acq. 12, both done with REC ordering. The unaccelerated long (7 sec) temporal footprint sequence (Acq. 10) and the short (2.6 sec) temporal footprint sequence with 2D SENSE acceleration of R = 4 have the same spatial resolution, while the accelerated scan had reduced image update times and temporal footprint. Each volunteer was imaged twice, once with each sequence, with a 10 minute delay for contrast clearance, with the first injection sequence chosen randomly for each volunteer. This allowed the two sequences to be compared on a volunteer-by-volunteer basis.

The second hypothesis (H2) was: for two view-shared sequences having equal frame rate and equal spatial resolution, the sequence with smaller temporal footprint will better portray the

temporal passage of the contrast bolus through the brain vasculature while retaining good overall image quality. The two sequences for this study are also identified in Table 1 as Acq. 13 and Acq. 11 respectively. EC ordering was used. Both sequences had image update times of just over 1 sec. The long (16 sec) temporal footprint sequence (Acq. 13) used an N16 CAPR sampling pattern with no SENSE acceleration. The short (3 sec) footprint sequence (Acq. 11) used an N3 pattern with 2D SENSE acceleration of $2.67 \times 2 = 5.33$. This hypothesis was tested similarly to that of H1 in five consecutive volunteers except each volunteer was imaged twice, once with each sequence, with no less than two days between the imaging sessions. This again allowed the two sequences to be compared on a volunteer-by-volunteer basis. The volunteers for testing H2 were different from those used for H1.

Evaluation

Data acquired from hypothesis H1 and H2 experiments spanning a time duration from prearterial enhancement to venous decay were reconstructed and transferred to a work station capable of displaying volumetric time series in both 2D sagittal source data, 2D axial and coronal reformats, as well as arbitrarily oriented maximum intensity projections (Advantage Windows; GE Medical Systems). Each time frame was sinc-interpolated to 1 mm^3 isotropic resolution. Evaluation was performed using eight different criteria as indicated in Table 2. For each criterion numerical scores were defined from 1 to 5, with 5 indicating the best performance. The criteria were selected so as to test for the desired temporal fidelity but also take into account potential artifact and other inadequacies. The evaluation was done in consensus by the two collaborating neuroradiologists (NGC, JH), having eight and 17 years of experience in neuro MRI, respectively. Since each volunteer was imaged with a corresponding pair of CAPR sequences, the associated evaluation scores could be compared on a volunteer-by-volunteer basis using statistical paired-difference approaches (51). Significance was tested using the Wilcoxon signed rank test within a commercial software package (JMP, version 6.0.0, 2005; SAS, Cary, NC) with significance taken to be $p < 0.05$.

RESULTS

Figure 4 shows the results of numerical simulations for sequences described in Table 1. Fig. 4A compares the performance of unaccelerated (Acq. 2) and R=2 (Acq. 4) and R=4 SENSE-accelerated CAPR (Acq. 7) sequences in portraying the reference carotid arterial waveform using the EC view order. Fig. 4B is a similar comparison for the REC order. Fig. 4C is a comparison of an EC, R=4 accelerated acquisitions for several different numbers of vane groups and illustrates the tradeoff between image update time and temporal footprint for fixed acceleration and unaccelerated reference scan (Acq. 2, 5, 7, 8, 10).

Table 3A summarizes the differences of the long versus short temporal footprint sequences tested by Hypothesis H1. The short temporal footprint sequence was markedly better to a statistically significant degree for arterial to venous separation (Category 5) as well as for ringing and ghosting artifact (Categories 1–2) and overall image quality (Category 8). Figure 5 is taken from one of the studies of Hypothesis H1 and illustrates the benefits of 2D acceleration in time-resolved acquisition. Fig. 5A shows successive sagittal MIPs from an N4 unaccelerated acquisition (Acq. 10). Fig. 5B shows for the same volunteer R=4 2D SENSE N4 results (Acq. 12). The 1.30 sec frame of (B) shows improved distal arterial filling than the 0.0 sec frame of (A) and with no filling of the superior sagittal sinus.

Table 3B summarizes the evaluation of Hypothesis H2 which compared two sequences with equal frame rate and spatial resolution. The short footprint case was rated superior in performance in arterial to venous separation (Category 5) and ringing and ghosting (Categories 1–2) to a statistically significant degree. In other categories differences were not significant. Figure 6 compares the temporal and spatial fidelity of the N16 (Acq. 11) and N3 (Acq. 13)

sequences tested by Hypothesis H2. Successive oblique MIPs of early arterial phase are shown in Fig. 6A thru Fig. 6C for the N16 sequence. Targeted sagittal MIPs of early and late venous phase are demonstrated in Fig. 6D and Fig. 6E. Similarly, Fig. 6F–J show corresponding results from the N3 sequence at the same times.

To provide improved spatial resolution of 1 mm^3 isotropic the sequence was further modified (Acq. 15 of Table 1). Oblique MIPs of the arterial and venous frames are shown in Figure 7A–B respectively. For this sequence central k-space was sampled in 0.988 sec, the update time was 3.09 sec, and the temporal footprint was 12.34 sec.

DISCUSSION

This work demonstrates a 3D MR angiographic technique based on Cartesian sampling, view sharing, and 2D SENSE acceleration which can image the whole brain with 1 to 2 mm isotropic spatial resolution, with sufficient temporal fidelity to resolve the intracranial arterial and venous phases of a gadolinium bolus. The arterial and venous phases can be clearly distinguished with image update times of one second or less and a temporal footprint as short as three seconds. As part of the development the parameter “temporal footprint” was introduced for characterization of sequences used for time-resolved imaging. In general, for a fixed spatial resolution in an echo-shared sequence there is a tradeoff between frame time and temporal footprint, as shown in the individual curves of Fig. 3. Incorporation of acceleration techniques such as 2D SENSE can reduce both the frame time and the temporal footprint which moves the performance point towards the origin of Fig. 3. Reduction of the temporal footprint by use of robust acceleration methods provides improved fidelity in the portrayal of a time-varying phenomenon. This was seen in the simulation results of Figs. 4A–B and corroborated in *in vivo* CE-MRA studies of the vasculature of the brain; e.g. in Fig. 5. As footprint increases due to increased view sharing there is some minor degradation of fidelity (Fig. 4C).

The construct of temporal footprint was introduced as a measure of the extent over which data are acquired for formation of an image in a view-shared sequence. Temporal footprint should not be equated with temporal response. Rather, temporal footprint can be used to assess the chance of non-idealities to interfere with the reconstructed image or the appropriateness for a specific application. For example, the temporal footprint of a sequence can be compared with breathhold duration to assess potential breathing artifact in thoracoabdominal imaging. As another example, in multi-station peripheral MRA it is often necessary to limit the acquisition time at proximal stations to 10–20 sec in order to track the advancing contrast bolus distally (52–54). Sequences with temporal footprints appreciably longer than this might not be practical in this application. Temporal footprint for view-shared, time-resolved sequences is akin to the acquisition time for cine acquisitions. Such times can range from minutes (55) to breathhold (56) to real-time (57), with tradeoffs of breathing artifact and SNR for each, while all providing sub-second temporal resolution.

The CAPR technique has properties which we believe are desirable for time-resolved sequences, simply stated as a consistency of temporal footprint for all frames. With the original view-shared technique (26,35) a sequential view order was used with a sliding window. Although the footprint duration was constant, the position of the central views within the window was variable and in some cases duplicated, leading to artifactual double images (e.g. Fig. 3D of Ref. (26)). For the keyhole technique (27) the peripheral views used for image formation are measured only once, either at the beginning or end of data acquisition, leading to temporal footprints with progressively longer or smaller duration. With the TRICKS method (28) the position of the central views within the temporal footprint varies, causing an object moving at fixed velocity to appear to have non-constant velocity in the image series. Moreover, interpolation of measurements of the central views (the “A” regions of Fig. 2 of Ref (28))

causes the reconstructed image to be a superposition of the states of the object at the measurement times of the central views, blunting the actual behavior. With the TREAT approach (Fig. 1 of Ref. (31)), the central views are acquired consistently every frame; however the center is elongated in time. With CAPR the temporal footprint duration is identical for all frames. Moreover, for each frame the k-space center is sampled only once and at the same point within the footprint, causing objects moving with constant velocity or which are changing their signal at a constant rate to be accurately portrayed as such in the reconstructed time frames. Study of this was beyond the scope of this work, but a sense of this can be seen in the leading edge of the contrast bolus in the left occipital artery in Figs. 6F–H (arrows).

The SNR performance of this sequence at these accelerations is robust. In this work the mean noise levels of the accelerated images were judged radiologically to be between Moderate and Minor (Table 3A–B, Category 4), and, while inferior to those of the unaccelerated images, not significantly so. This SNR robustness is due to several reasons. As discussed in the original 2D SENSE work (13), g-factors are markedly smaller in 2D vs. 1D SENSE. In a study of non-time-resolved CE-MRA of the brain we have shown that for 2D SENSE accelerations as high as 5.2 at 3.0 T, 75% of the g-factors were no larger than 2.08 (Fig. 5 and Table 3 of Ref. (58)). Moreover, 2D SENSE g-factors are highly consistent from subject-to-subject (59). Finally, 2D SENSE-accelerated time-resolved CE-MRA with EC view ordering benefits to some degree from the signal amplification effect of the non-time-resolved case (59).

Figure 3 can be used to provide some guidance as to the degree to which central k-space should be more frequently sampled than the k-space periphery. As seen, converting a sequence in which all views are sampled at the same frequency (N1) to one in which central k-space is sampled twice as frequently as the periphery (N2) provides a near two-fold reduction in frame time with only a minimal increase in temporal footprint. In fact, for the curves shown the N4 case for each was judged to be a good operating point, an effective tradeoff between a desirable short frame time and short temporal footprint. For high degrees of view sharing; e.g. the N16 case of Fig. 6A–E, the temporal footprint becomes undesirably prolonged, and the updating of only a limited extent of peripheral k-space can cause artifactual, directionally-dependent streaking and ghosting. The convexity of the curves of Fig. 3 will vary from those shown dependent on the size of the central k-space sampled, the orange disk of Fig. 1.

The value of SENSE acceleration technique was illustrated in a specific study (H1) in which subjects were imaged with two CAPR sequences, each having the same spatial resolution but an approximate three-fold difference in both frame time and temporal footprint. The improved ability of the small temporal footprint sequence to distinguish contrast arrival at different points in the intracranial vasculature was proven in a statistically significant manner (Category 5, Table 3A–B). Moreover, the overall image quality of the four-fold 2D SENSE accelerated CAPR was rated significantly higher as compared to the reference unaccelerated case (Category 8, Table 3A).

The effect of the duration of the temporal footprint on image quality was investigated in a second study (H2) comparing two time-resolved sequences which had identical frame time and spatial resolution but different temporal footprints. The long-footprint, N16 sequence resulted in markedly blunted portrayal of bolus dynamics vs. the short-footprint, accelerated N3 sequence. Moreover, the extensive level of view sharing of the N16 sequence was seen to cause artifactual blurring and ghosting due to the very limited degree to which peripheral k-space was updated with each new time frame (e.g. arrow, Fig. 6D; Categories 1–2, Table 3B). The 5.3-fold 2D SENSE acceleration allowed the N3 sequence to more accurately portray arterial and venous bolus dynamics and demonstrate higher overall image quality, Fig. 3B Category 8, than the unaccelerated N16 scan. This indicates that increasing the frame rate by using view sharing is not equivalent to increasing the frame rate by incorporation of SENSE.

In summary, we have described an acquisition method for providing time-resolved contrast-enhanced angiograms, and we have also presented the construct of temporal footprint for characterization of view-shared sequences. With respect to the first, the CAPR acquisition can be used with 2D SENSE accelerations as high as 5.3 to provide clear distinction of the arterial and venous phases of the whole brain with 1 to 2 mm isotropic spatial resolution, frame times as small as sub-second, and temporal footprints from 3 to 12 seconds, all while retaining high image quality. With respect to the second, the temporal footprint provides an objective measure of the extent over which data are used in image formation. The duration of and distribution of views within the footprint can potentially affect performance.

Acknowledgements

The authors would like to acknowledge the assistance of Kristina Schmidtknecht and Roger Grimm.

REFERENCES

1. Prince MR, Yucel EK, Kaufman JA, Harrison DC, Geller SC. Dynamic gadolinium-enhanced three-dimensional abdominal MR arteriography. J Magn Reson Imaging 1993;3:877–881. [PubMed: 8280977]
2. Zhang H, Maki JH, Prince MR. 3D contrast-enhanced MR angiography. J Magn Reson Imaging 2007;25:13–25. [PubMed: 17154188]
3. Schneider, G.; Prince, MR.; Meaney, JFM.; Ho, VB., editors. Magnetic Resonance Angiography: Techniques, Indications and Practical Applications. Milan: Springer; 2005.
4. Wilman AH, Riederer SJ. Improved centric phase encoding orders for three-dimensional magnetization-prepared MR angiography. Magn Reson Med 1996;36:384–392. [PubMed: 8875408]
5. Earls JP, Rofsky NM, DeCorato DR, Krinsky GA, Weinreb JC. Hepatic arterial-phase dynamic gadolinium-enhanced MR imaging: optimization with a test examination and a power injector. Radiology 1997;202:268–273. [PubMed: 8988222]
6. Foo TK, Saranathan M, Prince MR, Chenevert TL. Automated detection of bolus arrival and initiation of data acquisition in fast, three-dimensional, gadolinium-enhanced MR angiography. Radiology 1997;203:275–280. [PubMed: 9122407]
7. Wilman AH, Riederer SJ, King BF, Debbins JP, Rossman PJ, Ehman RL. Fluoroscopically triggered contrast-enhanced three-dimensional MR angiography with elliptical centric view order: application to the renal arteries. Radiology 1997;205:137–146. [PubMed: 9314975]
8. Peters DC, Korosec FR, Grist TM, Block WF, Holden JE, Vigen KK, Mistretta CA. Undersampled projection reconstruction applied to MR angiography. Magn Reson Med 2000;43:91–101. [PubMed: 10642735]
9. Barger AV, Block WF, Toropov Y, Grist TM, Mistretta CA. Time-resolved contrast-enhanced imaging with isotropic resolution and broad coverage using an undersampled 3D projection trajectory. Magn Reson Med 2002;48:297–305. [PubMed: 12210938]
10. Feinberg DA, Hale JD, Watts JC, Kaufman L, Mark A. Halving MR imaging time by conjugation: demonstration at 3.5 kG. Radiology 1986;161:527–531. [PubMed: 3763926]
11. Sodickson DK, Manning WJ. Simultaneous acquisition of spatial harmonics (SMASH): fast imaging with radiofrequency coil arrays. Magn Reson Med 1997;38:591–603. [PubMed: 9324327]
12. Pruessmann KP, Weiger M, Scheidegger MB, Boesiger P. SENSE: sensitivity encoding for fast MRI. Magn Reson Med 1999;42:952–962. [PubMed: 10542355]
13. Weiger M, Pruessmann KP, Boesiger P. 2D SENSE for faster 3D MRI. Magma 2002;14:10–19. [PubMed: 11796248]
14. Griswold MA, Jakob PM, Heidemann RM, Nittka M, Jellus V, Wang J, Kiefer B, Haase A. Generalized autocalibrating partially parallel acquisitions (GRAPPA). Magnetic Resonance in Medicine 2002;47:1202–1210. [PubMed: 12111967]
15. Sodickson DK, McKenzie CA, Li W, Wolff S, Manning WJ, Edelman RR. Contrast-enhanced 3D MR angiography with simultaneous acquisition of spatial harmonics: A pilot study. Radiology 2000;217:284–289. [PubMed: 11012458]

16. Weiger M, Pruessmann KP, Kassner A, Roditi G, Lawton T, Reid A, Boesiger P. Contrast-enhanced 3D MRA using SENSE. J Magn Reson Imaging 2000;12:671–677. [PubMed: 11050636]
17. Maki JH, Wilson GJ, Eubank WB, Hoogeveen RM. Utilizing SENSE to achieve lower station sub-millimeter isotropic resolution and minimal venous enhancement in peripheral MR angiography. J Magn Reson Imaging 2002;15:484–491. [PubMed: 11948840]
18. Wilson GJ, Hoogeveen RM, Willinek WA, Muthupillai R, Maki JH. Parallel imaging in MR angiography. Top Magn Reson Imaging 2004;15:169–185. [PubMed: 15479999]
19. Born M, Willinek WA, Gieseke J, von Falkenhausen M, Schild H, Kuhl CK. Sensitivity encoding (SENSE) for contrast-enhanced 3D MR angiography of the abdominal arteries. J Magn Reson Imaging 2005;22:559–565. [PubMed: 16161084]
20. Wilson GJ, Eubank WB, Vasbinder GB, Kessels AG, Hoogeveen RM, Muthupillai R, Maki JH. Utilizing SENSE to reduce scan duration in high-resolution contrast-enhanced renal MR angiography. J Magn Reson Imaging 2006;24:873–879. [PubMed: 16941607]
21. Hu HH, Madhuranthakam AJ, Kruger DG, Glockner JF, Riederer SJ. Combination of 2D sensitivity encoding and 2D partial fourier techniques for improved acceleration in 3D contrast-enhanced MR angiography. Magn Reson Med 2006;55:16–22. [PubMed: 16342155]
22. Nael K, Villablanca JP, Pope WB, McNamara TO, Laub G, Finn JP. Supraaortic arteries: contrast-enhanced MR angiography at 3.0 T--highly accelerated parallel acquisition for improved spatial resolution over an extended field of view. Radiology 2007;242:600–609. [PubMed: 17255428]
23. Xu PJ, Yan FH, Wang JH, Lin J, Fan J. Utilizing generalized autocalibrating partial parallel acquisition (GRAPPA) to achieve high-resolution contrast-enhanced MR angiography of hepatic artery: initial experience in orthotopic liver transplantation candidates. Eur J Radiol 2007;61:507–512. [PubMed: 17169520]
24. Schoenberg SO, Bock M, Knopp MV, Essig M, Laub G, Hawighorst H, Zuna I, Kallinowski F, van Kaick G. Renal arteries: optimization of three-dimensional gadolinium-enhanced MR angiography with bolus-timing-independent fast multiphase acquisition in a single breath hold. Radiology 1999;211:667–679. [PubMed: 10352590]
25. Finn JP, Baskaran V, Carr JC, McCarthy RM, Pereles FS, Kroeker R, Laub GA. Thorax: low-dose contrast-enhanced three-dimensional MR angiography with subsecond temporal resolution--initial results. Radiology 2002;224:896–904. [PubMed: 12202730]
26. Riederer SJ, Tasciyan T, Farzaneh F, Lee JN, Wright RC, Herfkens RJ. MR fluoroscopy: technical feasibility. Magn Reson Med 1988;8:1–15. [PubMed: 3173063]
27. van Vaals JJ, Brummer ME, Dixon WT, Tuithof HH, Engels H, Nelson RC, Gerety BM, Chezmar JL, den Boer JA. "Keyhole" method for accelerating imaging of contrast agent uptake. J Magn Reson Imaging 1993;3:671–675. [PubMed: 8347963]
28. Korosec FR, Frayne R, Grist TM, Mistretta CA. Time-resolved contrast-enhanced 3D MR angiography. Magn Reson Med 1996;36:345–351. [PubMed: 8875403]
29. Fink C, Ley S, Kroeker R, Requardt M, Kauczor HU, Bock M. Time-resolved contrast-enhanced three-dimensional magnetic resonance angiography of the chest: combination of parallel imaging with view sharing (TREAT). Invest Radiol 2005;40:40–48. [PubMed: 15597019]
30. Nael K, Fenchel M, Salamon N, Duckwiler GR, Laub G, Finn JP, Villablanca JP. Three-dimensional cerebral contrast-enhanced magnetic resonance venography at 3.0 Tesla: initial results using highly accelerated parallel acquisition. Invest Radiol 2006;41:763–768. [PubMed: 16971800]
31. Cashen TA, Carr JC, Shin W, Walker MT, Futterer SF, Shaibani A, McCarthy RM, Carroll TJ. Intracranial time-resolved contrast-enhanced MR angiography at 3T. AJNR Am J Neuroradiol 2006;27:822–829. [PubMed: 16611772]
32. Frydrychowicz A, Bley TA, Winterer JT, Harloff A, Langer M, Hennig J, Markl M. Accelerated time-resolved 3D contrast-enhanced MR angiography at 3T: clinical experience in 31 patients. Magma 2006;19:187–195. [PubMed: 16937136]
33. Gauvrit JY, Law M, Xu J, Carson R, Sunenshine P, Chen Q. Time-resolved MR angiography: optimal parallel imaging method. AJNR Am J Neuroradiol 2007;28:835–838. [PubMed: 17494652]
34. Mende KA, Froehlich JM, von Weymarn C, Hoogeveen R, Kistler T, Zollikofer CL, Wentz KU. Time-resolved, high-resolution contrast-enhanced MR angiography of dialysis shunts using the

CENTRA keyhole technique with parallel imaging. J Magn Reson Imaging 2007;25:832–840. [PubMed: 17345633]

35. Hadizadeh DR, von Falkenhausen M, Gieseke J, Meyer B, Urbach H, Hoogeveen R, Schild HH, Willinek WA. Cerebral arteriovenous malformation: Spetzler-Martin classification at subsecond-temporal-resolution four-dimensional MR angiography compared with that at DSA. Radiology 2008;246:205–213. [PubMed: 17951352]
36. Taschner CA, Gieseke J, Le Thuc V, Rachdi H, Reyns N, Gauvrit JY, Leclerc X. Intracranial arteriovenous malformation: time-resolved contrast-enhanced MR angiography with combination of parallel imaging, keyhole acquisition, and k-space sampling techniques at 1.5 T. Radiology 2008;246:871–879. [PubMed: 18195381]
37. Du J, Carroll TJ, Brodsky E, Lu A, Grist TM, Mistretta CA, Block WF. Contrast-enhanced peripheral magnetic resonance angiography using time-resolved vastly undersampled isotropic projection reconstruction. J Magn Reson Imaging 2004;20:894–900. [PubMed: 15503332]
38. Zhu H, Buck DG, Zhang Z, Zhang H, Wang P, Stenger VA, Prince MR, Wang Y. High temporal and spatial resolution 4D MRA using spiral data sampling and sliding window reconstruction. Magn Reson Med 2004;52:14–18. [PubMed: 15236361]
39. Mistretta CA, Wieben O, Velikina J, Block W, Perry J, Wu Y, Johnson K. Highly constrained backprojection for time-resolved MRI. Magn Reson Med 2006;55:30–40. [PubMed: 16342275]
40. Golay X, Brown SJ, Itoh R, Melhem ER. Time-resolved contrast-enhanced carotid MR angiography using sensitivity encoding (SENSE). AJNR Am J Neuroradiol 2001;22:1615–1619. [PubMed: 11559518]
41. Gauvrit JY, Leclerc X, Oppenheim C, Munier T, Trystram D, Rachdi H, Nataf F, Pruvo JP, Meder JF. Three-dimensional dynamic MR digital subtraction angiography using sensitivity encoding for the evaluation of intracranial arteriovenous malformations: a preliminary study. AJNR Am J Neuroradiol 2005;26:1525–1531. [PubMed: 15956525]
42. Ziyeh S, Strecker R, Berlis A, Weber J, Klisch J, Mader I. Dynamic 3D MR angiography of intra- and extracranial vascular malformations at 3T: a technical note. AJNR Am J Neuroradiol 2005;26:630–634. [PubMed: 15760877]
43. Meckel S, Mekle R, Taschner C, Haller S, Scheffler K, Radue EW, Wetzel SG. Time-resolved 3D contrast-enhanced MRA with GRAPPA on a 1.5-T system for imaging of craniocervical vascular disease: initial experience. Neuroradiology 2006;48:291–299. [PubMed: 16532336]
44. Hadizadeh DR, Gieseke J, Hoogeveen R, von Falkenhausen M, Meyer B, Urbach H, Schild H, Willinek WA. 4D Time-resolved angiography with CENTRA keyhole (4D-TRAK) and SENSE using a total acceleration factor of 60 as compared with catheter angiography in patients with cerebral arteriovenous malformations at 3.0T. Proc Joint Ann Mtg ISMRM-ESMRMB 2006:807.
45. Haider CR, Hu HH, Madhuranthakam AJ, Kruger DG, Campeau NG, Huston J 3rd, Riederer SJ. Time-resolved 3D contrast-enhanced MRA with 2D homodyne and view sharing for contrast bolus dynamics of the brain. Proc Joint Ann Mtg ISMRM-ESMRMB 2006:812.
46. Madhuranthakam AJ, Hu HH, Barger AV, Haider CR, Kruger DG, Glockner JF, Huston J 3rd, Riederer SJ. Undersampled elliptical centric view-order for improved spatial resolution in contrast-enhanced MR angiography. Magn Reson Med 2006;55:50–58. [PubMed: 16315207]
47. Noll DC, Nishimura DG, Macovski A. Homodyne Detection in Magnetic resonance Imaging. IEEE TMI 1991;10:154–163.
48. Wilman AH, Riederer SJ. Performance of an elliptical centric view order for signal enhancement and motion artifact suppression in breath-hold three-dimensional gradient echo imaging. Magn Reson Med 1997;38:793–802. [PubMed: 9358454]
49. Shankaranarayanan A, Wendt M, Aschoff AJ, Lewin JS, Duerk JL. Radial keyhole sequences for low field projection reconstruction interventional MRI. J Magn Reson Imaging 2001;13:142–151. [PubMed: 11169817]
50. Busse RF, Kruger DG, Debbins JP, Fain SB, Riederer SJ. A flexible view ordering technique for high-quality real-time 2DFT MR fluoroscopy. Magn Reson Med 1999;42:69–81. [PubMed: 10398952]
51. Rosner B. Fundamentals of Biostatistics. Duxbury Thomson Learning 2000:338–343.

52. Prince MR, Chabra SG, Watts R, Chen CZ, Winchester PA, Khilnani NM, Trost D, Bush HA, Kent KC, Wang Y. Contrast material travel times in patients undergoing peripheral MR angiography. Radiology 2002;224:55–61. [PubMed: 12091662]

53. Klessen C, Hein PA, Huppertz A, Voth M, Wagner M, Elgeti T, Kroll H, Hamm B, Taupitz M, Asbach P. First-pass whole-body magnetic resonance angiography (MRA) using the blood-pool contrast medium gadofosveset trisodium. Invest Radiol 2007;42:659–664. [PubMed: 17700282]

54. Du J, Korosec FR, Wu Y, Grist TM, Mistretta CA. Whole-body MR angiography using variable density sampling and dual-injection bolus-chase acquisition. Magn Reson Imag 2008;26:181–187.

55. Glover, GH.; Pelc, NJ. A rapid gated cine MRI technique. In: Kressel, HY., editor. Magnetic Resonance Annual 1988. New York: Raven Press; 1988. p. 299-333.

56. Atkinson DJ, Edelman RR. Cineangiography of the heart in a single breath hold with a segmented turboFLASH sequence. Radiology 1991;178:357–360. [PubMed: 1987592]

57. Kerr AB, Pauly JM, Hu BS, Li KC, Hardy CJ, Meyer CH, Macovski A, Nishimura DG. Real-time interactive MRI on a conventional scanner. Magn Reson Med 1997;38:355–367. [PubMed: 9339436]

58. Hu HH, Haider CR, Campeau NG, Huston J 3rd, Riederer SJ. Intracranial contrast-enhanced magnetic resonance venography with 6.4-fold sensitivity encoding at 1.5T and 3.0T. Journal of Magnetic Resonance Imaging. 2008In Press

59. Riederer SJ, Hu HH, Kruger DG, Haider CR, Campeau NG, Huston J 3rd. Intrinsic signal amplification in the application of 2D SENSE parallel imaging to 3D contrast-enhanced elliptical centric MRA and MRV. Magn Reson Med 2007;58:855–864. [PubMed: 17969124]

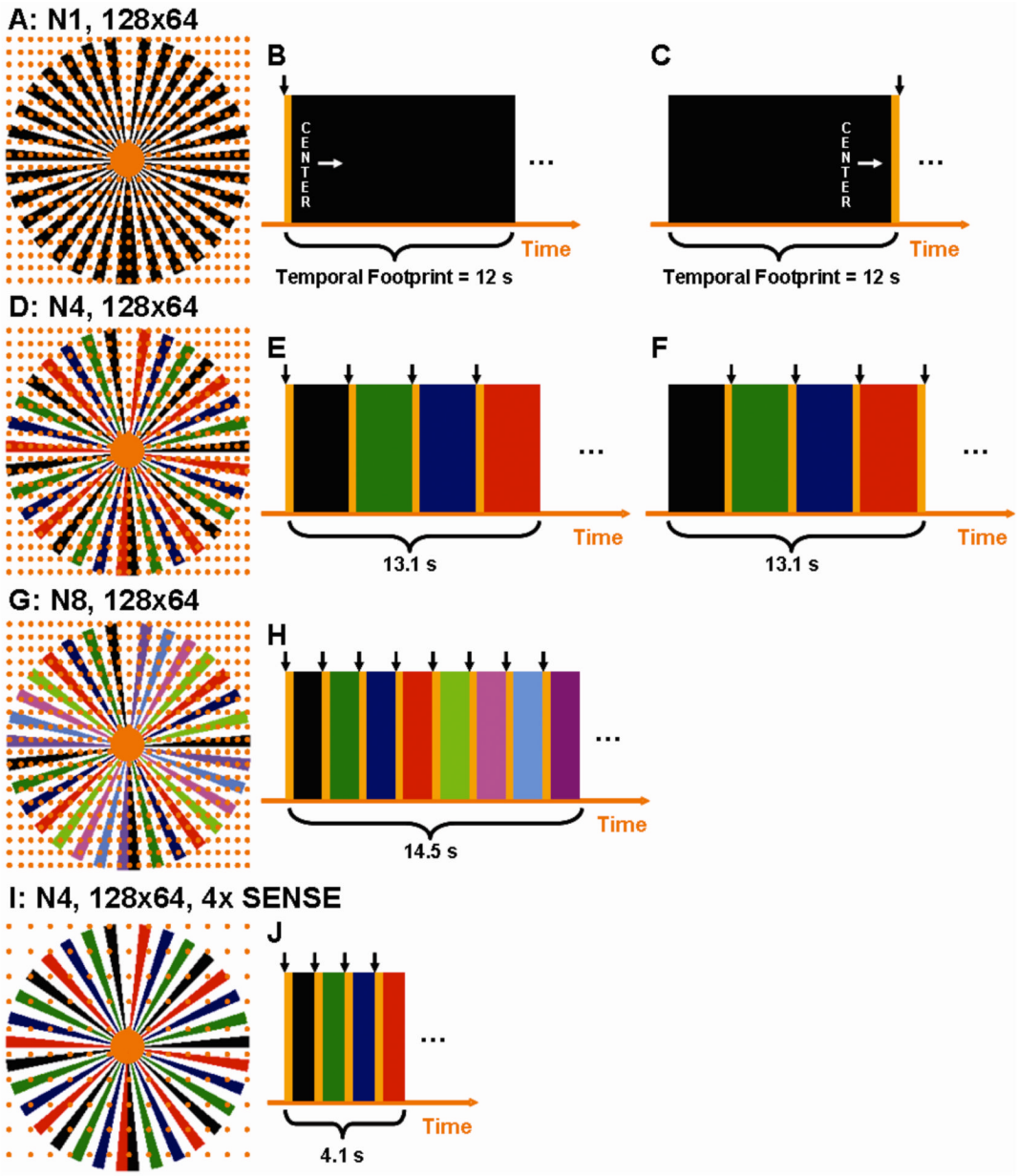

Figure 1.

A. The k_Y–k_Z phase encoding plane of the basic sampling pattern. B.–C. The temporal playout of the k-space pattern in 1A with elliptical centric (EC) encoding (B) and with reverse elliptical centric (REC) encoding (C). The black arrow indicates the point of reconstruction. D. The extension of 1A to four-fold view-sharing. E and F show the REC and EC temporal playout with four-fold view sharing. G. Higher degree of view sharing resulting from dividing the outer annulus into eight sets of vanes while (H) shows the decreased time between image updates and redundant sampling of k-space. I. Incorporation of 2D 4× SENSE into the pattern of (D). J. Temporal playout of the time-resolved 2D SENSE acquisition.

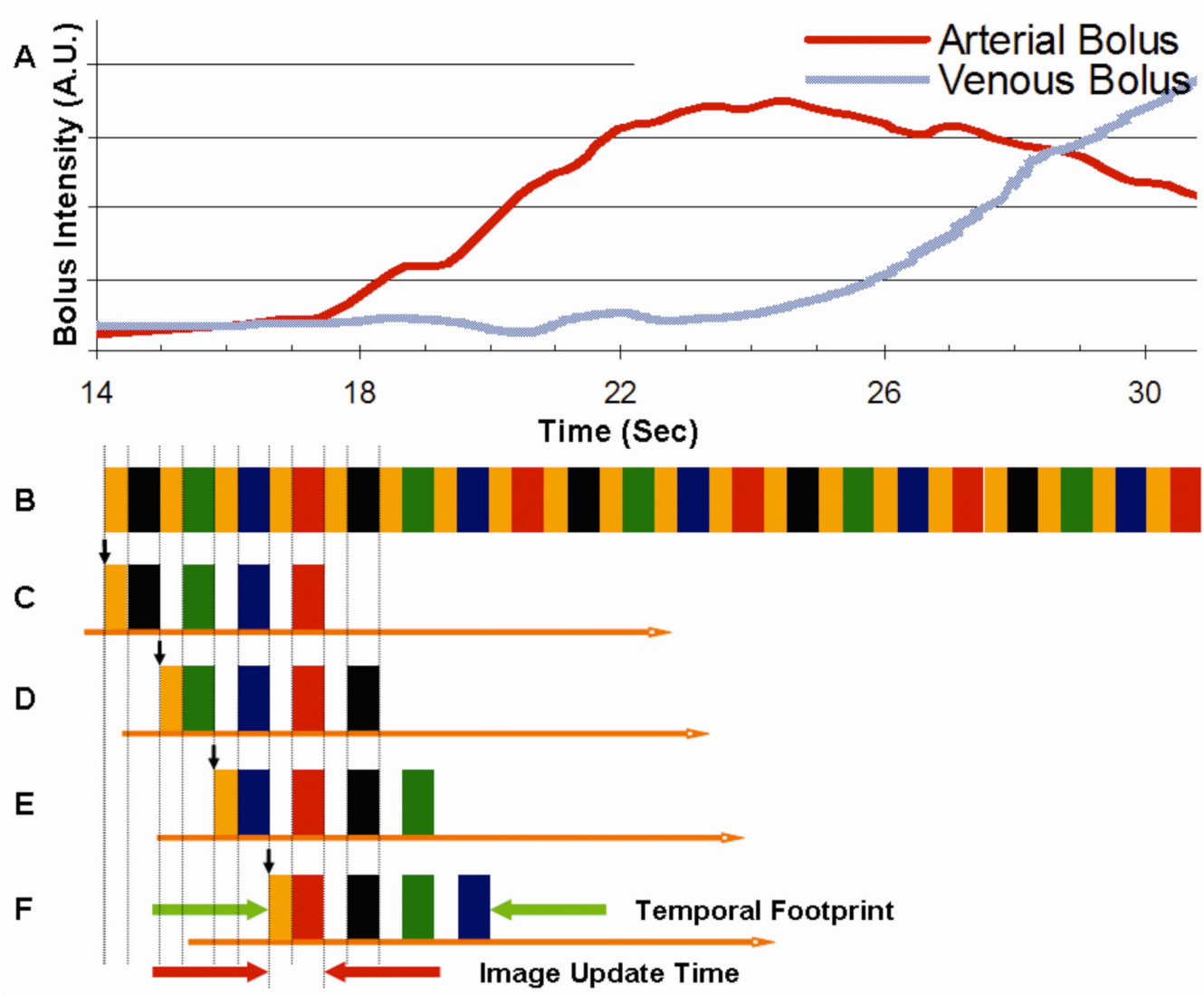

Figure 2.

A schematic showing (A) hypothetical arterial and venous contrast bolus time intensity profiles; (B) Extended playout of sampling pattern of Fig. 1D; (C–F) Selection of view playout of (B) indicating which data are used to reconstruct the first four timeframes. Vertical arrow for each indicates the time to which the corresponding image is assigned. Timings shown approximately correspond to Acq. 14 of Table 1.

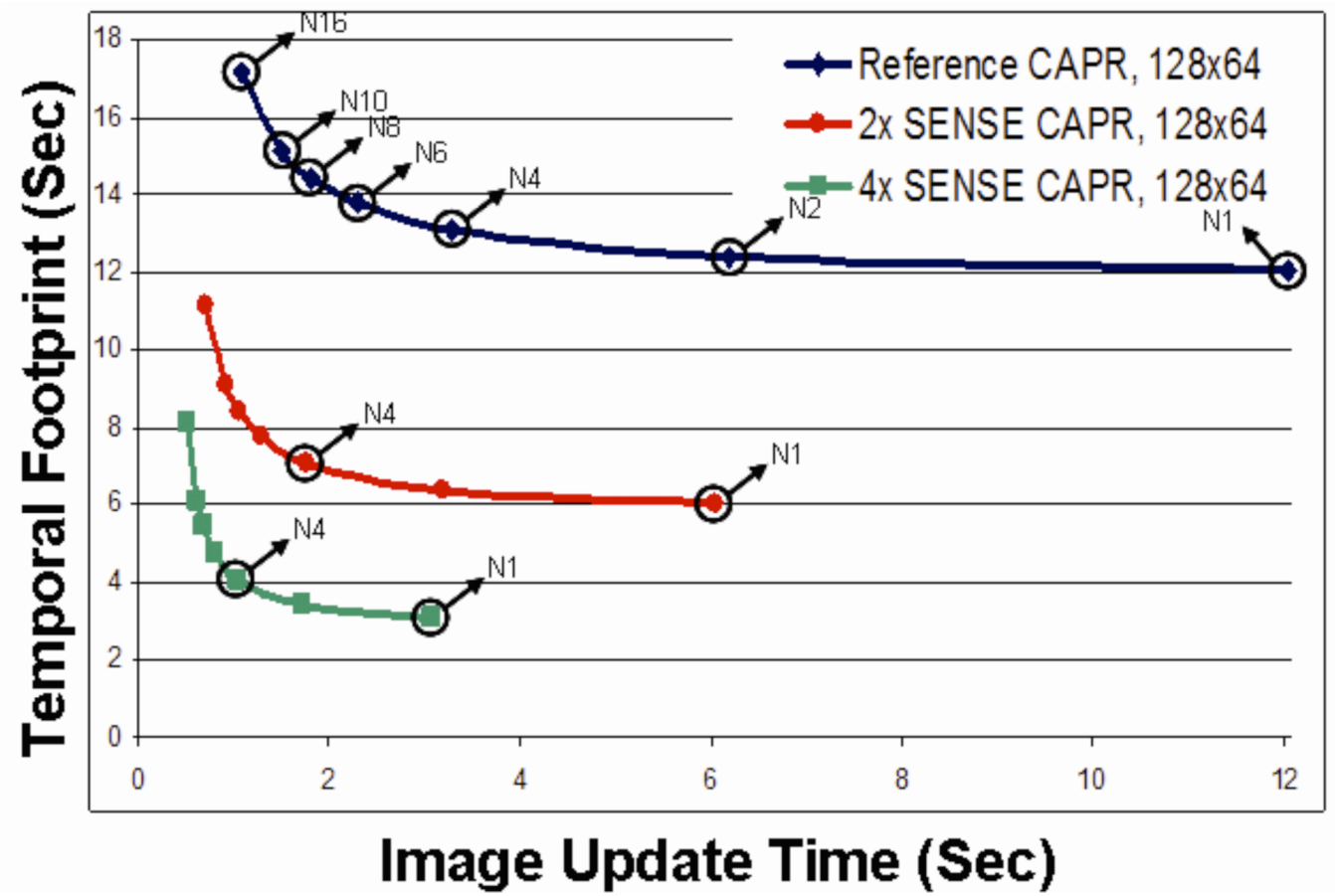

Figure 3.
Plot of temporal footprint vs. image update time. Points along a given curve indicate the number of sets of spokes used in the acquisition (N1, N2, etc.). The incorporation of 2× and 4× SENSE creates additional curves shifted towards the origin.

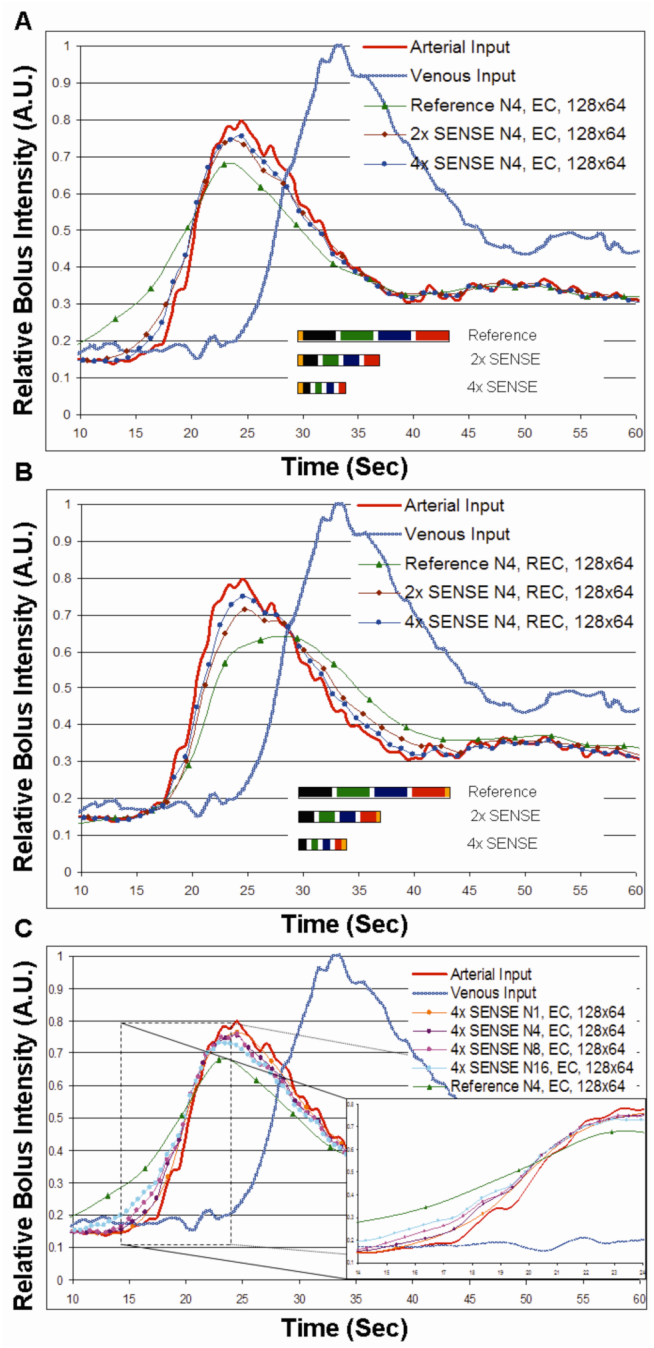

Figure 4.

A. Numerical simulations demonstrating temporal fidelity as a function of temporal footprint of a (i) reference N4, elliptical centric (EC) encoded, 128×64 CAPR sampling pattern (Table 1, Acq. 2) as compared to (ii) two-fold (Table 1, Acq. 4) and (iii) four-fold SENSE (Table 1, Acq. 7) accelerated imaging of the same sequence. Temporal footprints of all three sequences are also shown to scale. B. Results similar to (A) except for reverse elliptical centric ordering. C. Numerical simulations demonstrating temporal fidelity as a function of temporal footprint of a (i) reference N4, EC, 128×64 (Table 1, Acq. 2) sampling pattern as compared to 4× SENSE accelerated imaging various levels of view sharing (Table 1, Acq. 5, 7, 8, and 9).

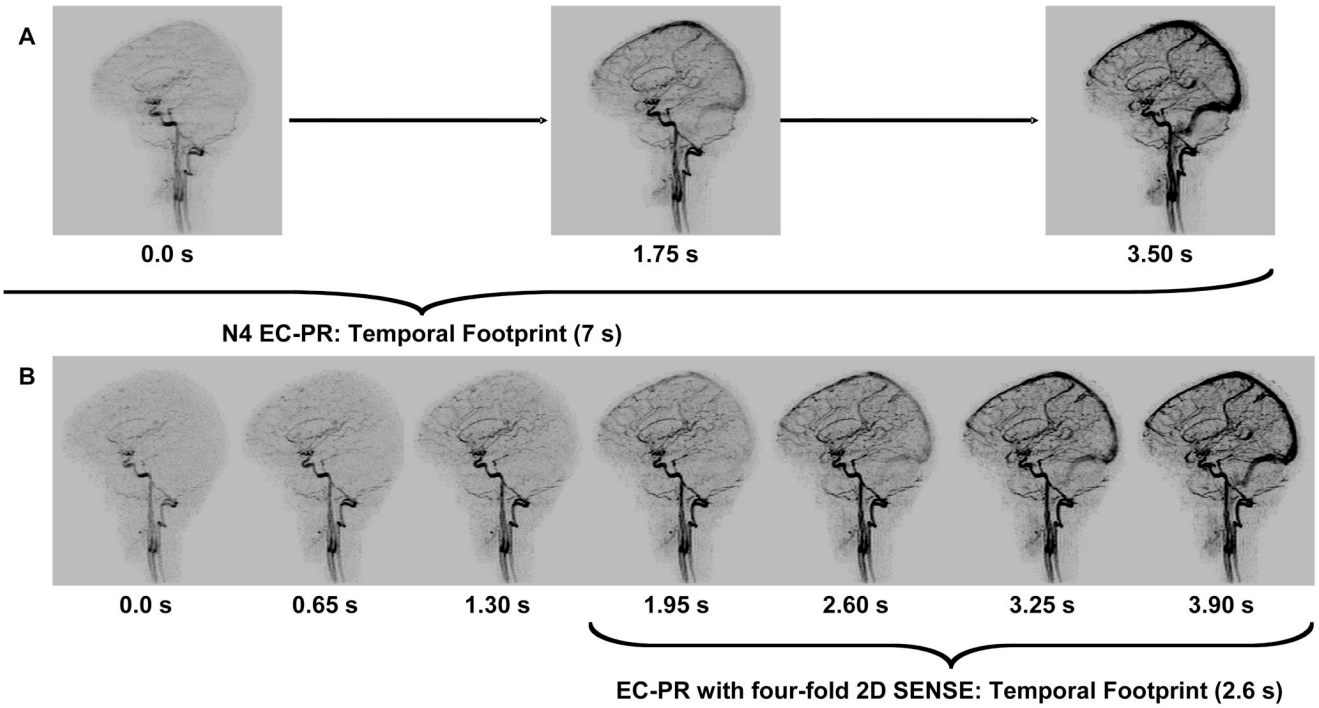

Figure 5.
MIPs for comparison of the image update time and temporal footprint for imaging with (A). N4 reference, reverse elliptical centric (REC) sequence (Table 1., Acq. 10) and (B) N4, four-fold SENSE accelerated, REC (Table 1., Acq. 12) sampling.

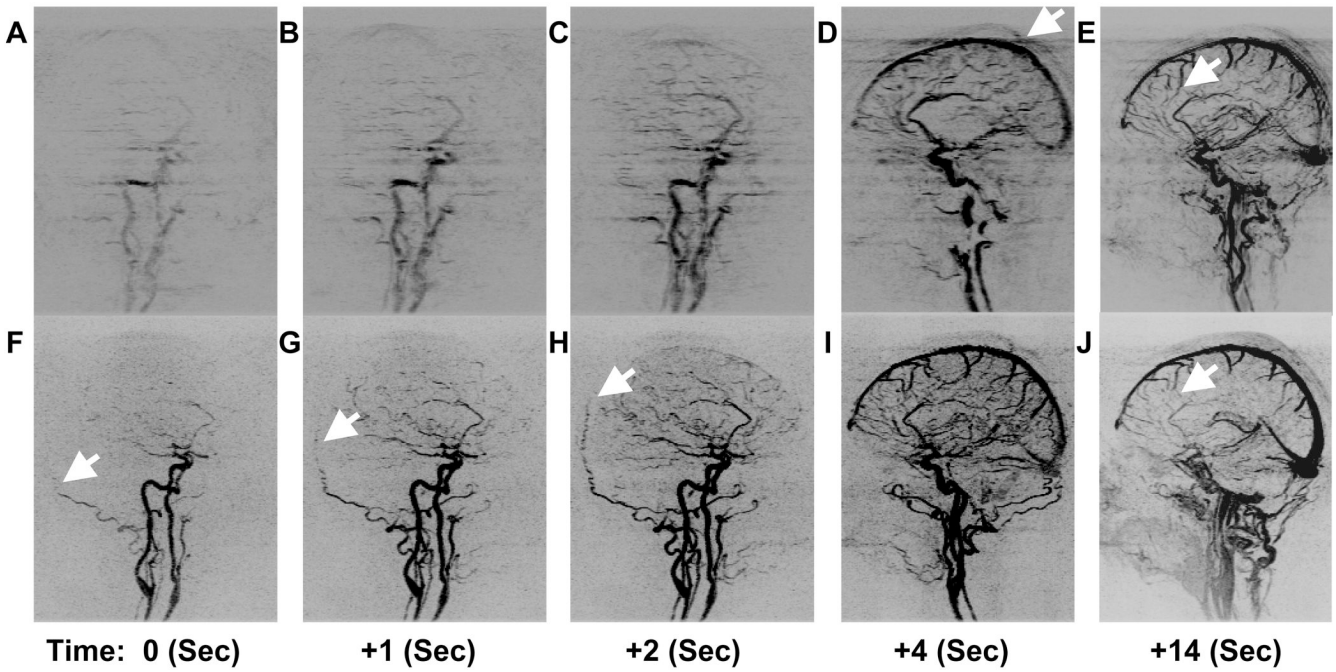

Figure 6.

Time series of images starting showing arterial opacification with three consecutive oblique MIPs (A–C), (D) a sagittal MIP two frames later, and a late venous phase targeted sagittal MIP (E) for an unaccelerated N16 sequence (Table 1, Acq. 11). Also shown are the corresponding frames for a 5.3-fold 2D SENSE accelerated N3 sequence (Table 1, Acq. 13). The arrow in (D) illustrates the blurring and ghosting caused by high view sharing acceleration. The arrows in Fig. F-G-H highlight progressive filling of the left occipital artery. The higher quality of small veins can be seen by the arrows in the N16 sequence (E) as compared to the N3 sequence (J).

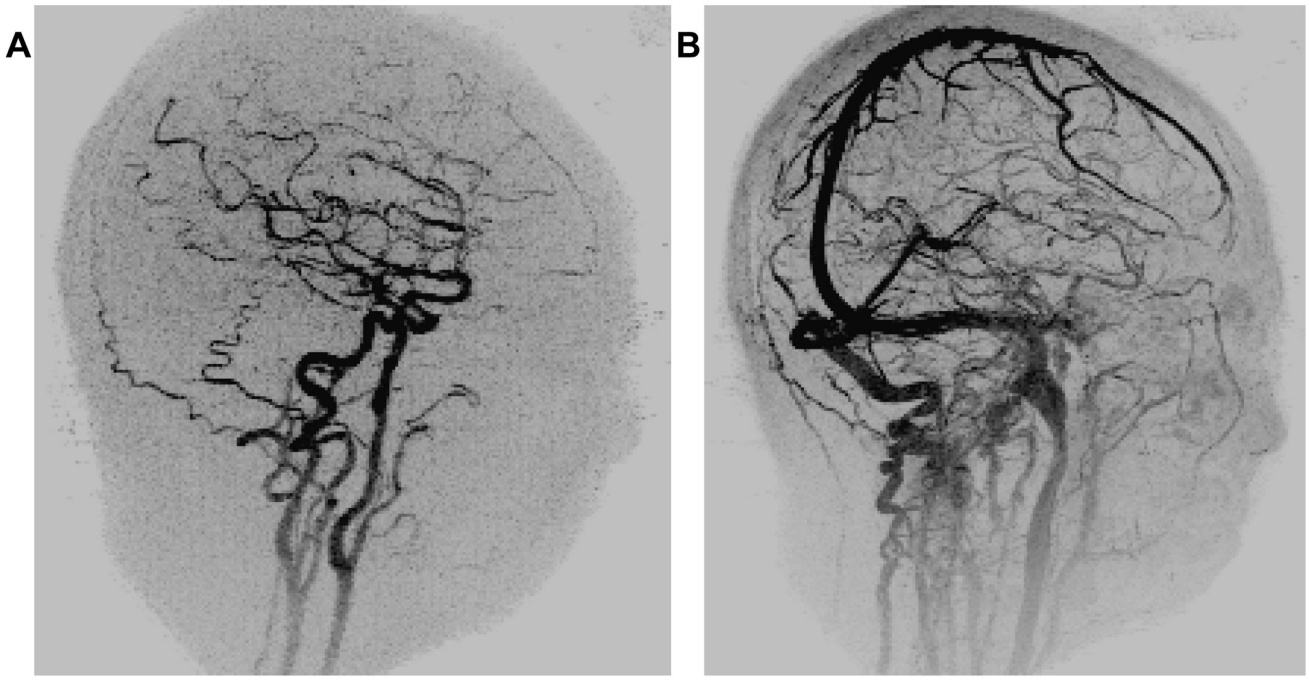

Figure 7.
Oblique views of A .an arterial phase and B. venous phase 12 seconds later with $1mm^3$ isotropic spatial resolution (Table 1, Acq. 15).

Table 1

Summary of CAPR sequences. Sampling resolution (Y × Z) shown is prior to any reduction provided by the SENSE acceleration. For all cases the X sampling resolution was 256 using a full echo.

Acq. #	No. of. Vane Sets	Sampling Resolution	Spatial Resolution	Center Update Time(Sec)	Image Update Time(Sec)	Temporal Footprint (Sec)	Figure #
	Numerical Experiments						
	Reference CAPR						
1	N1	128×64	1×2×2 mm^3	0.342	12.06	1×(12.06) = 12.06	1A–C, 3
2	N4	128×64	1×2×2 mm^3	0.342	3.27	4×(3.2718) = 13.09	1D–F, 3, 4A–C
3	N8	128×64	1×2×2 mm^3	0.342	1.81	8×(1.805) = 14.44	1G–H, 3
	2× CAPR						
4	N4	128×64	1×2×2 mm^3	0.342	1.77	4×(1.767) = 7.07	3, 4A
	4× CAPR						
5	N1	128×64	1×2×2 mm^3	0.342	3.06	1×(3.0628) = 3.06	4C
6	N2	128×64	1×2×2 mm^3	0.342	1.70	2×(1.7024) = 3.40	4C
7	N4	128×64	1×2×2 mm^3	0.342	1.02	4×(1.0222) = 4.09	1I–J, 3, 4A–B
8	N8	128×64	1×2×2 mm^3	0.342	0.68	8×(0.6802) = 5.449	4C
9	N16	128×64	1×2×2 mm^3	0.342	0.51	16×(0.5902) = 9.449	4C
	In Vivo Studies						
	Reference CAPR						
10	N4	128×32	1×2×4-6 mm^3	0.468	1.75	4×(1.75) = 7.0	5A
11	N16	128×64	1×2×2 mm^3	0.342	1.00	16×(1) = 16	6
	4× CAPR						
12	N4	128×32	1×2×4-6 mm^3	0.342	0.65	4×(0.646) = 2.589	5B
	5.3× CAPR						
13	N3	128×64	1×2×2 mm^3	0.4218	1.00	3×(1) = 3	6
14	N4	128×64	1×2×2 mm^3	0.342	0.84	4×(0.836) = 3.34	2
15	N4	256×128	1×1×1 mm^3	0.988	3.09	4×(3.086) = 12.34	7

Table 2

Evaluation criteria for short versus long temporal footprint volunteer studies.

Category 1 - Ringing (Zipper like artifact at the level of the Superios Sagittal and Transverse Sinuses)
Score - Assessment
1 - Nondiagnostic
2 - Severe. Probably will interfere with diagnosis.
3 - Moderate. Can potentially confound diagnosis.
4 - Minor. Does not affect diagnosis.
5 - None
Category 2 - Ghosting (Structured replications of the vessels or scalp, most likely caused by undersampling)
1 - Nondiagnostic
2 - Severe. Probably will interfere with diagnosis.
3 - Moderate. Can potentially confound diagnosis.
4 - Minor. Does not affect diagnosis.
5 - None
Category 3 - Motion (Swallowing or head movement, e.g. rotation, nod, shake)
1 - Nondiagnostic
2 - Severe. Probably will interfere with diagnosis.
3 - Moderate. Can potentially confound diagnosis.
4 - Minor. Does not affect diagnosis.
5 - None
Category 4 - Noise (Overall noise in the reconstruction whether streaking artifact or noise amplification from SENSE reconstruction)
1 - Nondiagnostic
2 - Severe. Probably will interfere with diagnosis.
3 - Moderate. Can potentially confound diagnosis.
4 - Minor. Does not affect diagnosis.
5 - None
Category 5 - Arterial to Venous Separation
1 - Absent. Presence of venous enhancement throughout arterial filling.
2 - Mild. Eearly enhancement of some venous structures.
3 - Moderate. Arterial enhancement peaks before intense venous signal; persistence of arterial and venous vasculature.
4 - Good. Clear progression of arterial to venous phase with many clear arterial frames (persistence of venous and arterial vascularity).
5 - Excellent. Clear arterial and venous washout.
Category 6 - Small Vessel Detail (conspicuity of small, central cerebral arteries and veins)
1 - Unable to resolve small vessels
2 - Poor. Nondiagnostic, faint and highly segmented.
3 - Moderate. Faint with some segmenting.
4 - Good. Mild, faint and continuous.
5 - Excellent. Intense, approaching or equal to that of venous signal intensity.

Category 1 - Ringing (Zipper like artifact at the level of the Superios Sagittal and Transverse Sinuses)

Score - Assessment

Category 7 - Vessels to Background Conspicuity (related to noise, ringing, ghosting, motion; and presence of contrast in vessels, sharpness, and blur)

1 - Poor contrast

2 - Mild. Poor contrast between vessels and background. Only larger vessels well defined.

3 - Moderate. Large vessels well seen; moderate conspicuity of medium vessels, small vessels poorly seen.

4 - Good. A few small vessels may be obscured. Excellent conspicuity of medium and small vessels.

5 - Excellent. Can clearly delineate all vessels from background.

Category 8 - Overall Diagnostic Quality

1 - Nondiagnostic

2 - Poor quality

3 - Marginal

4 - Good

5 - Excellent

Table 3

Summary of evaluations of result testing Hypothesis H1 and H2. See Table 2 for an explanation of the meaning of scores in each category. A. results for H1. B. Results for H2. Results were obtained by consensus of two neuroradiologists.

A	**Category 1, Ringing‡**			**Category 2, Ghosting‡**			**Category 3, Motion***			**Category 4, Noise***		
Temporal Footprint	**7 s**	**2.6 s**	**Difference**	**7 s**	**2.6 s**	**Difference**	**7 s**	**2.6 s**	**Difference**	**7 s**	**2.6 s**	**Difference**
Volunteer 1	2	4	2	4	4.5	0.5	5	5	0	4	3.5	−0.5
Volunteer 2	2	4	2	4	4.5	0.5	5	5	0	4	2.5	−1.5
Volunteer 3	2	4	2	2.5	4	1.5	5	5	0	3.5	3.5	0
Volunteer 4	2	4.5	2.5	3	4	1	5	5	0	4	4	0
Volunteer 5	2.5	5	2.5	3.5	5	1.5	5	5	0	4	4.5	0.5
Volunteer 6	2	4.5	2.5	3	4.5	1.5	5	5	0	4	4.5	0.5
Test Value			21			21			0			−2
P-Value			0.016			0.016			0.500			0.500

	Category 5, A–V Separation‡			**Category 6, Small Vessel Detail***			**Category 7, Vessel to Background***			**Category 8, Overall Image Quality‡**		
Temporal Footprint	7 s	2.6 s	Difference	7 s	2.6 s	Difference	7 s	2.6 s	Difference	7 s	2.6 s	Difference
Volunteer 1	2	4.5	2.5	4	3	−1	3.5	3.5	0	3	4	1
Volunteer 2	2	4.5	2.5	3.5	3	−0.5	3.5	3.5	0	3	4	1
Volunteer 3	2	4.5	2.5	2.5	3	0.5	3	3.5	0.5	2.5	3.5	1
Volunteer 4	2	4	2	2.5	2.5	0	2.5	2.5	0	2.5	4	1.5
Volunteer 5	2	5	3	2	2.5	0.5	2.5	3.5	1	3	4.5	1.5
Volunteer 6	2.5	4	1.5	2.5	2	−0.5	3	3.5	0.5	3	3.5	0.5
Test Value			21			−5			6			21
P-Value			0.016			0.375			0.125			0.016

A	**Category 1, Ringing‡**			**Category 2, Ghosting‡**			**Category 3, Motion***			**Category 4, Noise***		
Temporal Footprint	**7 s**	**2.6 s**	**Difference**	**7 s**	**2.6 s**	**Difference**	**7 s**	**2.6 s**	**Difference**	**7 s**	**2.6 s**	**Difference**

B	Category 1, Ringing‡			Category 2, Ghosting‡			Category 3, Motion*			Category 4, Noise*		
Temporal Footprint	16 s	3 s	Difference	16 s	3 s	Difference	16 s	3 s	Difference	16 s	3 s	Difference
Volunteer 1	2	5	3	3.5	5	1.5	4.5	5	0.5	4	2.5	−1.5
Volunteer 2	2	4	2	2	4.5	2.5	5	5	0	4	3	−1
Volunteer 3	2	4.5	2.5	2	5	3	5	5	0	3.5	3	−0.5
Volunteer 4	2	5	3	1.5	5	3.5	5	5	0	3	4	1
Volunteer 5	3	4.5	1.5	2.5	4.5	2	5	5	0	4	3.5	−0.5
Test Value			15			15			1			−8
P-Value			0.031			0.031			0.500			0.188

	Category 5, A–V Separation‡			Category 6, Small Vessel Detail*			Category 7, Vessel to Background*			Category 8, Overall Image Quality†		
Temporal Footprint	16 s	3 s	Difference	16 s	3 s	Difference	16 s	3 s	Difference	16 s	3 s	Difference
Volunteer 1	1.5	4.5	3	2	1	−1	2	3	1	2	3	1
Volunteer 2	1.5	4.5	3	2.5	2.5	0	2	3	1	2	3	1
Volunteer 3	2	4.5	2.5	2.5	2.5	0	2	3	1	2	3	1
Volunteer 4	1	4	3	2.5	1.5	−1	2	2.5	0.5	1.5	3	1.5
Volunteer 5	1.5	4.5	3	3	1.5	−1.5	3	2	−1	2.5	2.5	0
Test Value			15			−6			8			10

A	Category 1, Ringing‡			Category 2, Ghosting‡			Category 3, Motion*			Category 4, Noise*		
Temporal Footprint	**7 s**	**2.6 s**	**Difference**	**7 s**	**2.6 s**	**Difference**	**7 s**	**2.6 s**	**Difference**	**7 s**	**2.6 s**	**Difference**
P-Value			0.031			0.125			0.188			0.062

Note - One-Sided Wilcoxon Signed Rank Test. A positive difference or a positive values of signed ranks tends to favor the SENSE accelerated CAPR technique to the standard CAPR technique.

*$P > 0.1$.

†$P > 0.05$.

‡$P < 0.05$ (Significant Difference).